studies, however, have established that calcite dissolution is surface-controlled (i.e., not mass transport–limited) at pH > 4 (17, 21), a condition that was nominally satisfied in our experiments. The prevalence of front instabilities when the system is constantly driven by the beam probe suggests that they represent a mode of mineral/water interface reaction dynamics at conditions far from equilibrium (19). These instabilities therefore represent a dynamical signature of the onset of transport limitations and other dissipative processes at mineral/water interfaces.

REFERENCES AND NOTES

1. Y. Politi, T. Arad, E. Klein, S. Weiner, L. Addadi, *Science* **306**, 1161–1164 (2004).
2. S. L. Brantley, in *Kinetics of Water-Rock Interaction*, S. L. Brantley, J. D. Kubicki, A. F. White, Eds. (Springer, New York, 2008), pp. 152–210.
3. D. Gebauer, A. Völkel, H. Cölfen, *Science* **322**, 1819–1822 (2008).
4. A. F. Wallace *et al.*, *Science* **341**, 885–889 (2013).
5. A. C. Lasaga, A. Luttge, *Science* **291**, 2400–2404 (2001).
6. P. M. Dove, N. Han, J. J. De Yoreo, *Proc. Natl. Acad. Sci. U.S.A.* **102**, 15357–15362 (2005).
7. M. H. Nielsen, S. Aloni, J. J. De Yoreo, *Science* **345**, 1158–1162 (2014).
8. N. de Jonge, F. M. Ross, *Nat Nanotechnol.* **6**, 695–704 (2011).
9. N. M. Schneider *et al.*, *J. Phys. Chem. C* **118**, 22373–22382 (2014).
10. Materials and methods are available as supplementary materials on Science Online.
11. N. Laanait *et al.*, *J. Synchrotron Radiat.* **21**, 1252–1261 (2014).
12. P. Fenter, C. Park, Z. Zhang, S. Wang, *Nat. Phys.* **2**, 700–704 (2006).
13. L. Chou, R. M. Garrels, R. Wollast, *Chem. Geol.* **78**, 269–282 (1989).
14. E. J. Hart, *Science* **146**, 19–25 (1964).
15. A. H. Samuel, J. L. Magee, *J. Chem. Phys.* **21**, 1080 (1953).
16. J. A. Elliot, D. R. McCracken, *Fusion Eng. Des.* **13**, 21–27 (1990).
17. L. N. Plummer, T. M. L. Wigley, D. L. Parkhurst, *Am. J. Sci.* **278**, 179–216 (1978).
18. R. Shiraki, P. A. Rock, W. H. Casey, *Aquat. Geochem.* **6**, 87–108 (2000).
19. C. Steefel, in *Kinetics of Water-Rock Interaction*, S. L. Brantley, J. D. Kubicki, A. F. White, Eds. (Springer, New York, 2008), pp. 545–589.
20. I. Prigogine, G. Nicolis, *J. Chem. Phys.* **46**, 3542–3550 (1967).
21. O. S. Pokrovsky, S. V. Golubev, J. Schott, *Chem. Geol.* **217**, 239–255 (2005).

NEURODEVELOPMENT

A mechanism for the segregation of age in mammalian neural stem cells

D. L. Moore,[1] G. A. Pilz,[1] M. J. Araúzo-Bravo,[2,3] Y. Barral,[4] S. Jessberger[1]*

Throughout life, neural stem cells (NSCs) generate neurons in the mammalian brain. Using photobleaching experiments, we found that during cell division in vitro and within the developing mouse forebrain, NSCs generate a lateral diffusion barrier in the membrane of the endoplasmic reticulum, thereby promoting asymmetric segregation of cellular components. The diffusion barrier weakens with age and in response to impairment of lamin-associated nuclear envelope constituents. Weakening of the diffusion barrier disrupts asymmetric segregation of damaged proteins, a product of aging. Damaged proteins are asymmetrically inherited by the nonstem daughter cell in embryonic and young adult NSC divisions, whereas in the older adult brain, damaged proteins are more symmetrically distributed between progeny. Thus, these data identify a mechanism of how damage that accumulates with age is asymmetrically distributed during somatic stem cell division.

Neural stem cells (NSCs) continue to give rise to new neurons throughout life in distinct areas of the mammalian brain, such as the hippocampal dentate gyrus (1). Adult neurogenesis results in exchange of hippocampal neurons over the human life span and has been implicated in hippocampus-dependent learning and memory (1, 2). Failing or altered neurogenesis has been associated with a number of neuropsychiatric diseases such as major depression and epilepsy (1). The number of neurons generated is dynamically regulated. Advancing age, for example, correlates with a decline in NSC proliferation and neurogenesis, suggesting that the capacity of self-renewing NSCs to generate progeny diminishes with age (3, 4). However, the cellular mechanisms governing long-term self-renewal of hippocampal NSCs and mediating the age-associated decline of their neurogenic potential remain unknown.

Budding yeast establish a lateral diffusion barrier during cell division in the membrane of the endoplasmic reticulum (ER) that functions in part to segregate senescence factors, such as extrachromosomal DNA circles and protein aggregates, asymmetrically between the mother and daughter cell, leading to similar behavior of daughter cells independent of the age (i.e., the number of cell divisions that had occurred prior) of the mother (5, 6). Asymmetric distribution of senescence factors has been also described in *Drosophila* somatic stem cells, as well as in mammalian cells such as human embryonic kidney (HEK) 293T cells and human embryonic stem cells (7–9). We asked whether asymmetric segregation of senescence factors is associated with diffusion barriers in mammalian cells.

To investigate whether rodent NSCs form a diffusion barrier in the ER membrane, we first used fluorescence loss in photobleaching (FLIP) experiments to visualize exchange of ER proteins between future daughter cells during cell division (10). We used green fluorescent protein (GFP)–tagged reporters of the ER lumen [using the ER-retrieval amino acid sequence Lys-Asp-Glu-Leu (KDEL); LumER-GFP] and the ER membrane (Sec61α; MemER-GFP) (10). NSCs expressed mCherry-tagged histone H2B to facilitate cell cycle stage identification. We performed FLIP experiments using NSCs isolated from the adult rat dentate gyrus, beginning in anaphase and continuing through the end of telophase. A small region was repetitively photobleached while the fluorescence intensity was measured in the two future daughter cells, separated by the cleavage plane (Fig. 1, A and B, and fig. S1A). Photobleaching of LumER-GFP resulted in a comparable loss of fluorescence in the bleached and unbleached daughter cells (Fig. 1, A, C, D, and F, fig. S1, A to C, and movie S1). In contrast, FLIP of MemER-GFP revealed loss of fluorescence up to the cleavage plane; the opposite daughter compartment was unaffected (Fig. 1, B, C, E, and F, fig. S1, A to C, and movie S2). The compartmentalized loss of fluorescence was not due to the distance of the photobleached area relative to the analyzed area, as bleaching regions medial to segregating chromosomes and close to the cleavage plane gave similar results (Fig. 1, G to J, fig. S1, D to I, and movies S3 and S4). Thus, NSCs establish a diffusion barrier relative to the cleavage plane that is present during cell division.

We next analyzed whether the strength of the underlying barrier is dynamically regulated with age. To confirm that in vitro aged NSCs retain some of their in vivo characteristics, we performed a 5-ethynyl-2´-deoxyuridine (EdU) pulse in hippocampal NSCs isolated from middle-aged (9-month-old) mice and young (1.5-month-old) mice. Analogous to the in vivo situation, aged NSCs in vitro were less proliferative than young

[1]Brain Research Institute, Faculty of Medicine and Science, University of Zürich, 8057 Zürich, Switzerland. [2]Biodonostia Health Research Institute, 20014 San Sebastián, Spain. [3]IKERBASQUE, Basque Foundation for Science, 48013 Bilbao, Spain. [4]Institute of Biochemistry, Department of Biology, ETH Zürich, 8093 Zürich, Switzerland.
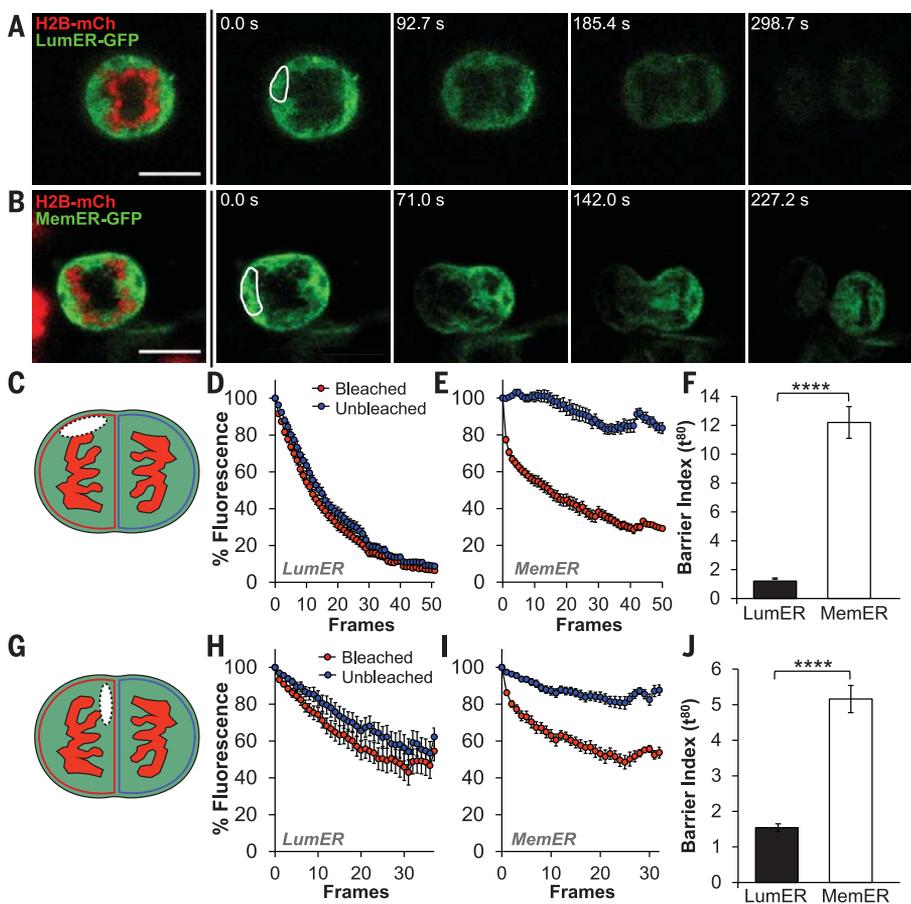*Corresponding author. E-mail: jessberger@hifo.uzh.ch

Fig. 1. Mammalian NSCs establish a lateral diffusion barrier based in the ER membrane during mitosis. (**A**) FLIP experiments in rat NSCs overexpressing LumER-GFP (green; targeted to ER lumen) or (**B**) MemER-GFP (green; targeted to ER membrane) with histone H2B-mCherry (red; DNA). Note the compartmentalized loss of fluorescence with MemER-GFP bleaching that occurs selectively on the bleached side of the dividing NSC. White outline indicates bleached region of interest (ROI). (**C**) Schematic illustrating the ROI (dashed line) repeatedly bleached in rat NSCs during time-lapse imaging for (D) to (F). Fluorescence was measured on each side of the presumptive cleavage plane throughout division, beginning in early to mid-anaphase. (**D** and **E**) Average fluorescence intensity at each time point in bleached (red) and unbleached (blue) compartments for LumER-GFP ($n = 19$ cells) (D) and MemER-GFP ($n = 18$ cells) (E); values are mean ± SEM. (**F**) Quantification of barrier strength at time $t = 80$ s derived from nonlinear fitted curves from (D) and (E) for LumER-GFP (black bar) and MemER-GFP (white bar; unpaired t test; mean ± SEM). (**G**) Schematic depicting the ROI (dashed line) for inner bleaching experiments used in (H) to (J). (**H** and **I**) Quantification of fluorescence loss over time for LumER-GFP ($n = 20$ cells) (H) and MemER-GFP ($n = 22$ cells) (I) when ROI is close to the cleavage plane (mean ± SEM). Bleaching began later in anaphase for an optimal ROI medial to the chromosomes, thus leading to shorter imaging length and reduced final values of total bleaching. (**J**) Quantification of barrier strength at $t = 80$ s based on fitted curves for LumER-GFP (black bar) and MemER-GFP (white bar) after inner ROI bleaching (unpaired t test; mean ± SEM). Scale bars, 10 μm. ****$P < 0.0001$.

NSCs (fig. S2, A to C). Old NSCs retained their neurogenic potential and showed gene expression profiles comparable to those of young NSCs (fig. S2, D and E, and table S1). However, in old NSCs, fluorescence substantially decreased not only in the bleached but also in the unbleached compartment upon continuous FLIP photobleaching of MemER-GFP (Fig. 2, A to E, and movies S6 and S8), indicating that the diffusion barrier weakens with age. Reduced ER compartmentalization in old NSCs was independent of potential age-associated alterations of cellular diffusion properties as measured by

fluorescence recovery after photobleaching (FRAP) of MemER-GFP (fig. S2, G to J) and was also independent of anaphase-telophase duration (fig. S2F). No difference was seen between old and young NSCs in LumER-GFP FLIP experiments (fig. S2, K to O, and movies S5 and S7). Thus, the strength of the diffusion barrier decreases with age in mouse NSCs.

We next aimed to identify the molecular requirements of the mouse diffusion barrier. We focused on lamin-associated components of the nuclear envelope that become part of the ER during mitosis in mammalian cells (*11*). To dis-

rupt lamin function in NSCs, we overexpressed a dominant-negative mutant form of lamin A called progerin that causes Hutchinson-Gilford progeria syndrome, a disease of premature aging (*12*). Retrovirus-mediated overexpression of progerin in young NSCs recapitulated the weakened diffusion barrier observed in old NSCs and led to reduced compartmentalization of fluorescence upon FLIP of MemER-GFP (Fig. 2, G, I, and J, fig. S3A, and movie S12), whereas control virus overexpression had no effect on the barrier (Fig. 2, F, H, and J, fig. S3A, and movie S10). The increased loss of fluorescence in the unbleached compartment in progerin-overexpressing cells was not due to a difference in the duration of anaphase-telophase (fig. S3B), nor to changes in the diffusion rate of MemER-GFP as measured by FRAP (fig. S3, C to F). Likewise, the dynamics of LumER-GFP were not altered by progerin overexpression (fig. S3, G to I, and movies S9 and S11). Progerin-mediated reduction in barrier strength was associated with decreased proliferation of young NSCs similar to that observed in old NSCs (fig. S3J). Thus, lamin-dependent mechanisms are required for proper barrier function and proliferation of cultured NSCs.

We next investigated whether NSCs establish a diffusion barrier when dividing within their endogenous niche. Because of the current technical limitations of imaging NSCs within their adult hippocampal niche, we switched to embryonic NSCs and electroporated embryonic day 13 (E13) mouse embryos with LumER-GFP or MemER-GFP constructs (*13*). Ex vivo slices were generated at E14, and longitudinal imaging of apical progenitors (radial glia NSCs) and basal progenitors, identified by mitotic positioning relative to the ventricular surface, began after 1 day in vitro. Because of the heterogeneity of proliferating NSCs in the developing cortex (*14*), we performed single-trace analyses of fluorescence intensity differences between the unbleached and bleached compartments for every cell upon FLIP experiments in apical and basal progenitors (fig. S4, A and B). FLIP of LumER-GFP showed no compartmentalization of fluorescence in either apical or basal progenitors (Fig. 3, A and C to F, fig. S4, A to F, and movies S15 and S18). Loss of fluorescence with MemER-GFP FLIP experiments was compartmentalized in 26% of the analyzed apical progenitors and 24% of the analyzed basal progenitors, whereas the remainder of the MemER-GFP apical and basal progenitors showed no diffusion barrier (Fig. 3, B to F, fig. S4, A to E, and movies S13, S14, S16, and S17). Thus, these findings reveal the existence of a diffusion barrier in subsets of apical progenitors and basal progenitors within their endogenous niche. Differential establishment of a diffusion barrier may contribute to the heterogeneity of apical and basal progenitors in the developing cortex (*14*).

We next asked which cellular components the barrier might segregate. In budding yeast, senescence factors such as damaged proteins and extrachromosomal DNA circles become asymmetrically segregated during division (*6*, *15*, *16*). Thus, we analyzed the distribution of ubiquitinated
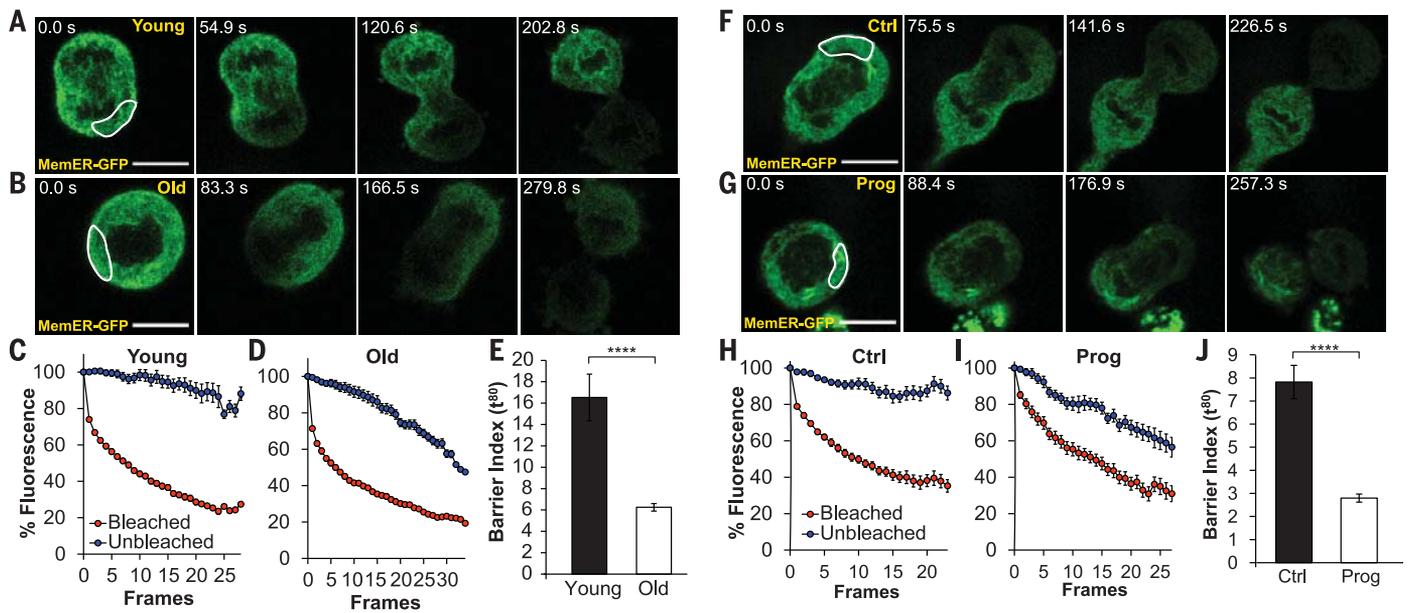
Fig. 2. The strength of the NSC diffusion barrier is weakened with age and overexpression of the lamin A mutant protein progerin. (**A** and **B**) Time course of fluorescence loss during FLIP of MemER-GFP (green) in young (A) and old (B) mouse NSCs. Note the loss of fluorescence in both compartments in old NSCs as compared to young. White outline indicates bleached ROI. (**C** and **D**) Quantification of fluorescence intensities in bleached (red) and unbleached (blue) compartments for MemER-GFP in young NSCs ($n = 35$ cells) (C) and old NSCs ($n = 35$ cells) (D); values are mean ± SEM. (**E**) Quantification of barrier strength of MemER-GFP at $t = 80$ s derived from nonlinear fitted curves from (C) and (D) (unpaired t test; mean ± SEM). (**F** and **G**)

Representative images of a time course of fluorescence loss during FLIP of MemER-GFP (green) in young NSCs transduced with control virus (F) or progerin (G). White outline indicates bleached ROI. (**H** and **I**) Quantification of fluorescence intensity in bleached (red) and unbleached (blue) compartments for MemER-GFP in young NSCs transduced with control virus ($n = 18$ cells) (H) and progerin ($n = 14$ cells) (I); values are mean ± SEM. Progerin overexpression results in reduced compartmentalization of fluorescence loss. (**J**) Quantification of the barrier strength of MemER-GFP at $t = 80$ s taken from nonlinear fitted curves created from (H) and (I) (unpaired t test; mean ± SEM). Scale bars, 10 μm. ****$P < 0.0001$.

Fig. 3. Subpopulations of NSCs in the developing mouse cortex possess a lateral diffusion barrier during mitosis. (**A** and **B**) Time course of fluorescence loss during FLIP of LumER-GFP (A) and MemER-GFP (B) in basal progenitor (BP) cells of the developing cortex (E14+1 day in vitro). Note the compartmentalized loss of fluorescence with MemER-GFP bleaching selectively on the bleached side of the dividing NSC. Dashed lines indicate the cell of interest; white outline indicates bleached ROI. (**C**) Single-cell fluorescence traces plotting the difference in fluores-

cence intensity between the unbleached and bleached compartment at each time point reveal a compartmentalized loss of fluorescence upon FLIP in this MemER-GFP$^+$ BP (B) but not the LumER-GFP$^+$ BP (A). (**D** and **E**) Averaged single cell traces of the difference in fluorescence intensity of MemER-GFP between unbleached and bleached compartments during FLIP for each imaged BP ($n = 21$ cells) (D) and apical progenitor (AP; $n = 13$ cells)
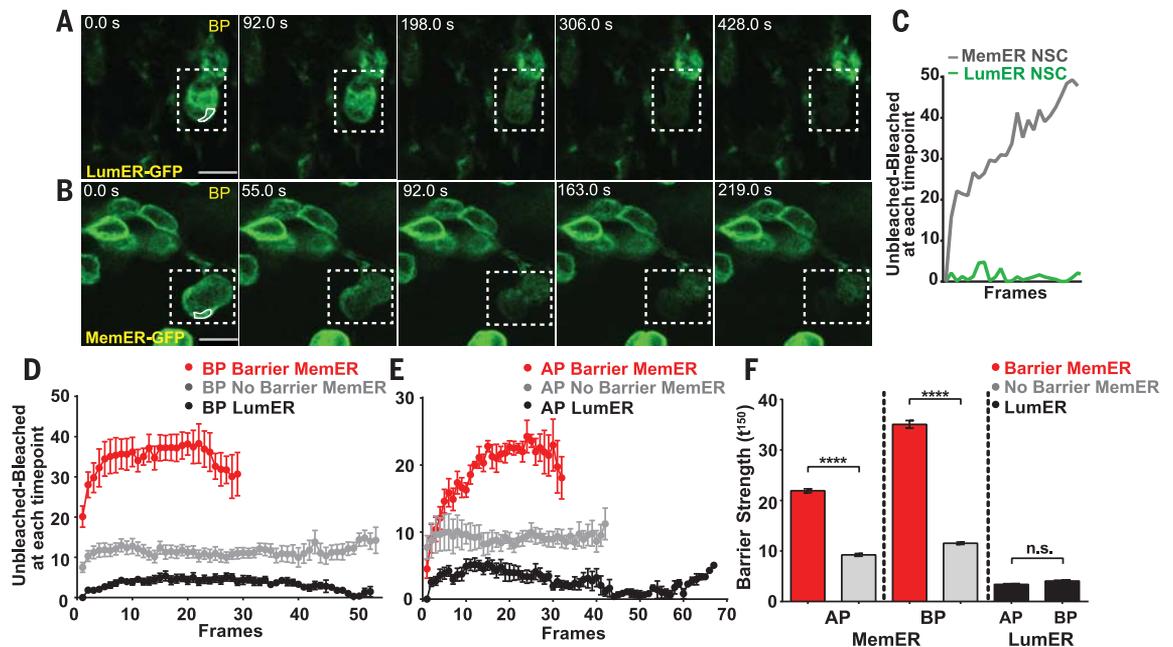
(E) reveal subpopulations that have barrier formation (red lines) and those with no barrier formation (gray lines) relative to LumER-GFP FLIP traces (black lines; $n = 9$ cells AP, $n = 12$ cells BP). (**F**) Quantification of barrier strength at $t = 150$ s derived from one-phase association fitted curves created from (D) and (E) (unpaired t test; mean ± SEM). Scale bars, 10 μm. ****$P < 0.0001$.
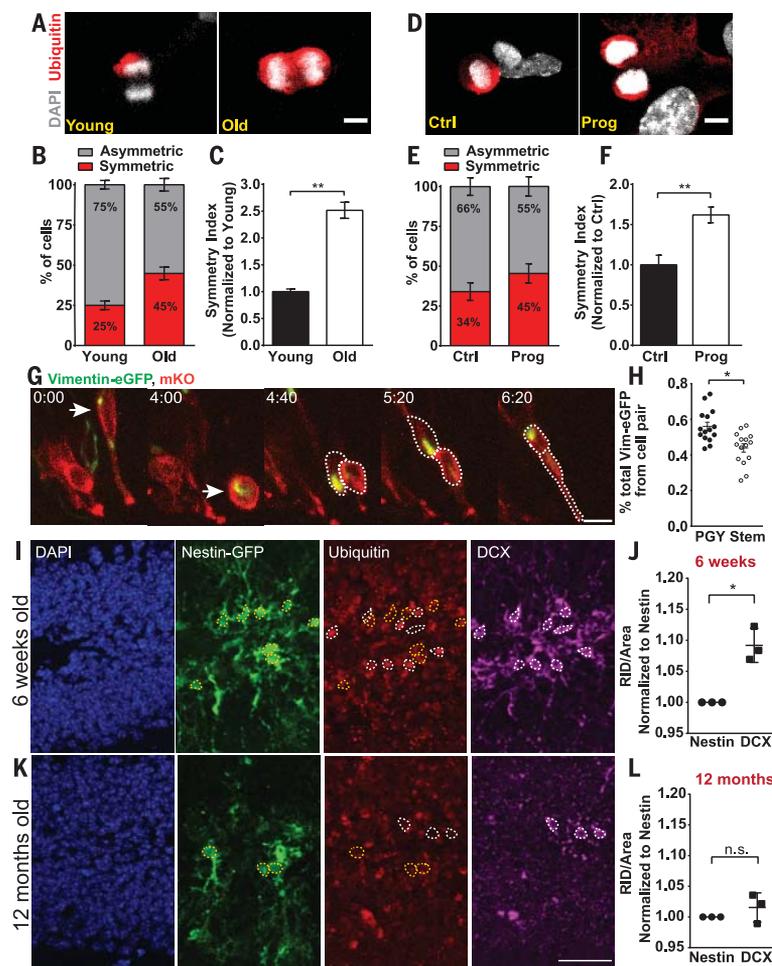
Fig. 4. Diffusion barrier strength is associated with the asymmetric segregation of damaged proteins that determine the cellular behavior of NSCs. (**A**) Ubiquitinated proteins (red) are asymmetrically distributed in young dividing NSCs (left) as compared to old NSCs (right). Nuclei were counterstained with 4′,6-diamidino-2-phenylindole (DAPI; gray). (**B**) Quantifications of symmetric (red) versus asymmetric (gray) distribution of ubiquitinated proteins in young (left) and old (right) NSCs (mean ± SEM). (**C**) A symmetry index ratio (see supplementary materials) revealed an increase in the number of old NSCs (white bar) with symmetric distribution of ubiquitinated proteins as compared to young NSCs (black bar) (unpaired t test; mean ± SEM). (**D**) Overexpression of progerin (right) led to a more symmetric distribution of ubiquitinated proteins relative to control virus (left). Nuclei were counterstained with DAPI (gray). (**E**) Quantifications of the symmetric (red) or asymmetric (gray) distribution of ubiquitinated proteins after control virus or progerin overexpression (mean ± SEM). (**F**) The symmetry index ratio normalized to control virus (black bar) revealed that progerin overexpression (white bar) increases the symmetric distribution of ubiquitinated proteins similarly to that of old NSCs (unpaired t test; mean ± SEM). Error bars on controls (Young or Ctrl) represent SEM of the original non-normalized values. (**G**) Apical progenitors overexpressing vimentin-eGFP to visualize localization of ubiquitinated proteins, and mKusabira Orange to visualize the cell outlines, were imaged in E15 mouse brain slices. The dividing NSC (arrow) and daughter cells (dashed lines) are indicated. (**H**) The intensity of vimentin-eGFP in each daughter cell was divided by the total amount of vimentin-eGFP between the two cells. The nonstem progeny (PGY, black circles) received more vimentin-eGFP at each division than did the stem daughter cell (cell that retained the apical process; empty circles) ($n = 15$ cell pairs; paired t test; mean ± SEM). (**I** and **K**) Nestin-GFP brains were stained against DAPI (nuclei; blue), GFP (stem cells; green), ubiquitinated proteins (Ub; red), and doublecortin (DCX; immature neurons; magenta) and imaged in 6-week-old (I) or 12-month-old (K) male mice. Outlines of confirmed cell bodies of nestin$^+$ cells (yellow outlines) and DCX$^+$ cells (white outlines) were overlaid onto the Ub channel to measure Ub intensities. (**J** and **L**) The raw integrated density (RID) of Ub was measured for each nestin-GFP$^+$ or DCX$^+$ cell body and normalized to its area before also normalizing to the background. Dots represent the averages from each animal that were normalized with nestin as 100%. In 6-week-old animals (J), DCX$^+$ cells had a significantly greater amount of Ub than in nestin$^+$ cells, whereas in 12-month-old mice (L), there was no statistical difference ($P = 0.3787$) between the two types of cells ($n = 3$ animals each; paired t test; mean ± SEM). Scale bars, 5 μm [(A) and (D)], 10 μm (G), 40 μm [(I) and (K)]. *$P < 0.05$, **$P < 0.01$.

proteins in dividing NSCs. As in mammalian stem cell populations in vitro and *D. melanogaster* embryos (*7, 8*), young mouse NSCs displayed asymmetric segregation of ubiquitin (indicative of protein damage) in late stages of mitosis (Fig. 4, A to C). This asymmetry was reduced in old NSCs (Fig. 4, A to C). Overexpression of progerin phenocopied the effect of aging and led to a more symmetric segregation of ubiquitinated proteins (Fig. 4, D to F). Thus, a weaker barrier correlates with more symmetric distribution of damaged proteins with age.

To elucidate the functional consequences of asymmetric segregation of damaged proteins in NSCs, we established a live sensor allowing for single-cell monitoring of damaged protein segregation. Because overexpression of the sensor GFP-ubiquitin (*17*) induced cell death in NSCs, we made use of the intermediate filament protein vimentin, which asymmetrically segregates with misfolded proteins during cell division (*9*). Immunostaining of vimentin and ubiquitin in young NSCs revealed asymmetric distribution of vimentin during late mitosis. Vimentin cosegregated with ubiquitin $95.5 ± 0.8\%$ of the time (fig. S5, A and B). Similarly, overexpressed vimentin-eGFP segregated asymmetrically in mitotic NSCs, cosegregating with endogenous ubiquitin $70.8 ± 0.9\%$ of the time (fig. S5, C to E), and was not toxic to the cells. Thus, we asked whether asymmetric segregation of vimentin-eGFP in young dividing NSCs is associated with cell cycle length. We measured asymmetry of vimentin-eGFP at the first anaphase and calculated the length of time until the next division for each daughter cell. In 63% of dyads ($P < 0.05$), the daughter NSC that received more vimentin-eGFP took longer to divide than its sister cell (fig. S5F and movie S19). Thus, for rodent NSCs as for human embryonic stem cells, HEK293T cells, and certain cancer cells (*7, 9*), ubiquitinated or damaged proteins reduce the rate of proliferation.

To analyze the asymmetric segregation of damaged proteins in situ, we electroporated E13 mouse embryos with vimentin-eGFP, performed slice cultures at E14, and began longitudinal imaging overnight. In apical progenitor divisions, the nonstem daughter cell inherited more vimentin-eGFP relative to the total amount of vimentin-eGFP, indicating that the stem cell gives away the ubiquitinated proteins to its more committed progeny (Fig. 4, G and H, and movie S20). This further supports the finding that NSCs that receive a greater amount of ubiquitinated proteins have a longer cell cycle duration, as the apical progenitor nonstem daughter cells have a lengthening of the cell cycle associated with fate restriction (*18*). To investigate damage segregation in the adult brain, we performed immunostaining on brain slices of nestin-GFP mice at 6 weeks and 12 months of age. Sections were stained with anti-doublecortin (to label newborn neurons), anti-ubiquitin (to label damaged proteins), and anti-GFP (to label hippocampal NSCs and amplify the nestin signal). Ubiquitin intensity was measured in the doublecortin$^+$ or nestin$^+$ cells. Doublecortin$^+$ cells had more ubiquitin

signal than nestin^{+} cells in 6-week-old mice (Fig. 4, I and J). At 12 months, however, ubiquitin levels were not significantly different between NSCs and their neuronal progeny (Fig. 4, K and L) despite the general increase in ubiquitin levels in the older brain (fig. S5G). These findings establish that NSCs retain fewer damaged proteins during cell division and support the hypothesis that weakening of the diffusion barrier with age contributes to the more symmetric segregation of ubiquitinated proteins between NSCs and their neuronal progeny in vivo.

Our results show how age affects protein segregation during mammalian NSC division by altering a diffusion barrier. The diffusion barrier facilitates asymmetric segregation of damaged proteins between daughter cells, keeping the self-renewed stem cell free from damage. As in yeast, young rodent NSCs efficiently compartmentalize cellular damage, protecting the proliferative cell. Age reduces the efficiency of this compartmentalization, exposing the aged NSCs to excess cellular damage. Examining the role of the ER diffusion barrier in other mammalian cells will determine whether this represents a general mechanism for the asymmetric segregation of damage during cell divisions of somatic stem cells or other immortal cells, such as cancer cells.

REFERENCES AND NOTES

1. K. M. Christian, H. Song, G. L. Ming, *Annu. Rev. Neurosci.* **37**, 243–262 (2014).
2. K. L. Spalding *et al.*, *Cell* **153**, 1219–1227 (2013).
3. M. A. Bonaguidi *et al.*, *Cell* **145**, 1142–1155 (2011).
4. H. G. Kuhn, H. Dickinson-Anson, F. H. Gage, *J. Neurosci.* **16**, 2027–2033 (1996).
5. L. Clay *et al.*, *eLife* **3**, e01883 (2014).
6. Z. Shcheprova, S. Baldi, S. B. Frei, G. Gonnet, Y. Barral, *Nature* **454**, 728–734 (2008).
7. L. C. Fuentealba, E. Eivers, D. Geissert, V. Taelman, E. M. De Robertis, *Proc. Natl. Acad. Sci. U.S.A.* **105**, 7732–7737 (2008).
8. M. R. Bufalino, B. DeVeale, D. van der Kooy, *J. Cell Biol.* **201**, 523–530 (2013).
9. M. Ogrodnik *et al.*, *Proc. Natl. Acad. Sci. U.S.A.* **111**, 8049–8054 (2014).
10. C. Luedeke *et al.*, *J. Cell Biol.* **169**, 897–908 (2005).
11. C. Wandke, U. Kutay, *Cell* **152**, 1222–1225 (2013).
12. T. Dechat *et al.*, *Genes Dev.* **22**, 832–853 (2008).
13. S. C. Noctor, A. C. Flint, T. A. Weissman, R. S. Dammerman, A. R. Kriegstein, *Nature* **409**, 714–720 (2001).
14. L. M. Farkas, W. B. Huttner, *Curr. Opin. Cell Biol.* **20**, 707–715 (2008).
15. H. Aguilaniu, L. Gustafsson, M. Rigoulet, T. Nyström, *Science* **299**, 1751–1753 (2003).
16. K. A. Henderson, D. E. Gottschling, *Curr. Opin. Cell Biol.* **20**, 723–728 (2008).
17. N. P. Dantuma, T. A. Groothuis, F. A. Salomons, J. Neefjes, *J. Cell Biol.* **173**, 19–26 (2006).
18. J. T. Paridaen, W. B. Huttner, *EMBO Rep.* **15**, 351–364 (2014).

DENGUE TYPING

Dengue viruses cluster antigenically but not as discrete serotypes

Leah C. Katzelnick,[1,2,3,4] Judith M. Fonville,[1,2,5] Gregory D. Gromowski,[3] Jose Bustos Arriaga,[3] Angela Green,[4] Sarah L. James,[1,2] Louis Lau,[4] Magelda Montoya,[4] Chunling Wang,[4] Laura A. VanBlargan,[3] Colin A. Russell,[6] Hlaing Myat Thu,[7] Theodore C. Pierson,[3] Philippe Buchy,[8] John G. Aaskov,[9,10] Jorge L. Muñoz-Jordán,[11] Nikos Vasilakis,[12,13,14] Robert V. Gibbons,[15] Robert B. Tesh,[12,13,14] Albert D.M.E. Osterhaus,[5] Ron A.M. Fouchier,[5] Anna Durbin,[16] Cameron P. Simmons,[17,18,19] Edward C. Holmes,[20] Eva Harris,[4] Stephen S. Whitehead,[3] Derek J. Smith[1,2,5]*

The four genetically divergent dengue virus (DENV) types are traditionally classified as serotypes. Antigenic and genetic differences among the DENV types influence disease outcome, vaccine-induced protection, epidemic magnitude, and viral evolution. We characterized antigenic diversity in the DENV types by antigenic maps constructed from neutralizing antibody titers obtained from African green monkeys and after human vaccination and natural infections. Genetically, geographically, and temporally, diverse DENV isolates clustered loosely by type, but we found that many are as similar antigenically to a virus of a different type as to some viruses of the same type. Primary infection antisera did not neutralize all viruses of the same DENV type any better than other types did up to 2 years after infection and did not show improved neutralization to homologous type isolates. That the canonical DENV types are not antigenically homogeneous has implications for vaccination and research on the dynamics of immunity, disease, and the evolution of DENV.

Dengue virus (DENV) infects up to 390 million people each year, and of the 96 million individuals who develop an acute systemic illness, ~500,000 experience potentially life-threatening complications, including hemorrhage and shock (*1*, *2*). The four genetic DENV types have long been thought to exist as four serotypes, and the antigenic differences between the types are believed to have a key role in the severity of disease, epidemic magnitude, viral evolution, and design of vaccines (*3–5*).

The description of DENV types as serotypes originated with the observation that the human immune response following primary DENV infection fully protected against challenge with viruses of the homologous type but only partially, and transiently, protected against challenge by viruses of a heterologous type (*6*). This finding was supported by in vitro neutralization experiments in which each DENV type was on average better neutralized by homologous than heterologous DENV infection antisera (*7*). The immune response immediately after a primary DENV infection varied from individual to individual, but generally was characterized by high titers of neutralizing antibodies to multiple DENV types. The neutralizing response was observed to become more DENV type–specific over time (*8*). It was later shown that antibodies to a heterologous DENV type could enhance infection in vivo and were associated with increased risk of severe disease in nature (*9*, *10*). Although antigenic variability was observed within DENV types from the earliest studies, this variation is generally considered to be substantially less than the differences between types, and not thought to modify type-specific protection (*11*, *12*). Together, the DENV types clearly form an antigenic subgroup within the genus *Flavivirus* (*13*, *14*). Analyses of envelope (E) proteins, and later full genomes, showed that the four types are as genetically divergent among themselves as sequences assigned to different viruses within the genus *Flavivirus* (*15*). These deep evolutionary divergences between DENV types were evident in the phylogenetic tree of the genetically diverse E-gene sequences of the viruses that we investigated here (Fig. 1A, fig. S1, and table S1) (*16*). Similarly, a map of amino acid differences between the E proteins revealed four compact, segregated types (Fig. 1B and fig. S2), as the number of amino acid substitutions between heterologous types far exceeded the maximum difference within a type.

However, investigations that rely on the classification of DENV into serotypes do not fully explain clinical and epidemiological phenomena.

The following resources related to this article are available online at www.sciencemag.org (this information is current as of September 23, 2015):

Updated information and services, including high-resolution figures, can be found in the online version of this article at:
http://www.sciencemag.org/content/349/6254/1334.full.html

Supporting Online Material can be found at:
http://www.sciencemag.org/content/suppl/2015/09/16/349.6254.1334.DC1.html

A list of selected additional articles on the Science Web sites **related to this article** can be found at:
http://www.sciencemag.org/content/349/6254/1334.full.html#related

This article **cites 34 articles**, 16 of which can be accessed free:
http://www.sciencemag.org/content/349/6254/1334.full.html#ref-list-1

This article appears in the following **subject collections:**
Development
http://www.sciencemag.org/cgi/collection/development